Ocean Modelling 69 (2013) 136–145

Contents lists available at SciVerse ScienceDirect

Ocean Modelling

journal homepage: www.elsevier.com/locate/ocemod

Roles of shelf slope and wind on upwelling: A case study off east and west coasts of the US

Zhaoyun Chen [a,d], Xiao-Hai Yan [a,b,d], Yuwu Jiang [a,d,*], Lide Jiang [c]

[a] State Key Laboratory of Marine Environmental Science, Xiamen University, Xiamen 361005, Fujian, China
[b] Center for Remote Sensing, College of Earth, Ocean and Environment, University of Delaware, Newark, DE 19716, USA
[c] NOAA/NESDIS/STAR, E/RA3, 5200 Auth Road, NOAA Science Center, Camp Springs, MD 20746, USA
[d] Joint Institute for Coastal Research and Management (UD/XMU Joint-CRM), USA

ARTICLE INFO

Article history:
Received 18 January 2013
Received in revised form 11 June 2013
Accepted 14 June 2013
Available online 28 June 2013

Keywords:
Upwelling age
Upwelling index
Shelf slope
Wind
Sea surface temperature
Numerical model

ABSTRACT

To understand the differences in upwelling tendency between the east and west coasts of the U.S., idealized numerical experiments were performed to examine the upwelling response to wind and shelf slope. The primary results show that steeper slope leads to narrower cross-shore width of surface Ekman divergence (WSED) and larger vertical velocity, while stronger upwelling favorable wind stress induces broader WSED and larger vertical velocity. Meanwhile, the wind duration is substantial to determine both the area and intensity of upwelling off the coast. The tendencies for cold upwelling areas off each coast are compared by the upwelling age, which is defined as the ratio of the duration of upwelling favorable wind to the advection time. The advection time, defined as the time scale for cold water to be advected from the pycnocline to the ocean surface, is improved to comprise of climbing time and upwelling time. The latter is related to the upwelling divergence driven by surface Ekman flow. The depth of the switch point of these two processes is approximately $0.9D_E$ (D_E is the Ekman depth). The proposed formula for the advection time is found to be consistent with estimates derived from the use of particle trajectory analysis within the numerical model results. The consideration of upwelling age shows that differences in wind forcing are more important than bottom slope in accounting for the different characteristics of upwelling areas off the California and New Jersey coasts.

1. Introduction

Upwelling is an important oceanographic phenomenon in coastal ecosystems because the onshore subsurface flow brings bottom nutrients up into the euphotic zone and leads to high concentrations of plankton and zooplankton. The development of cold upwelling area consists of two stages: (1) cold water advected from the pycnocline to the surface (the time scale of this process is known as the advection time (Jiang et al., 2012)); and (2) the upwelling front at the sea surface migrating offshore to form a large area of cold water off the coast. It is found that gentle slope is unfavorable for the wind-induced upwelling (Allen et al., 1994; Jiang et al., 2011). However, little work has been done (Jiang et al., 2012) to compare the upwelling systems off the California coast to those off the New Jersey coast regarding the wind and slope effects on coastal upwelling. Based on Ekman theory, Jiang et al. (2012) proposed a concept of "upwelling age", Γ, which is defined as wind duration, t_{wind}, divided by advection time t_{ad}, i.e. $\Gamma = t_{wind}/t_{ad}$. The advection time is the required time to advect the cold water from pycnocline to the coast, and is inversely proportional to wind stress and shelf slope. The advantage of this indicator to quantify the coastal upwelling is the multiple considerations of the effects of wind duration, shelf slope and wind strength, all of which are crucial factors in determining coastal upwelling tendency. In particular, we focus on the study of advection time, which is the primary part of the upwelling age quantifying the tendency for the development of a cold upwelling area, and seek to explain the significant differences that exist between the cold upwelling areas off these two coasts as observed in satellite sea surface temperature (SST) images.

The duration of the upwelling favorable wind plays an important role in the spatial extent of the upwelling and the amount of the temperature drop. The cold upwelling area is closely related to the time-integrated wind stress (Breaker and Mooers, 1986; Jiang et al., 2011). When the upwelling favorable wind weakens, the upwelling circulation relaxes, leading to reduced upwelling intensity and weaker alongshore currents (Melton et al., 2009; Pringle and Dever, 2009). In addition to the effects of the wind, the bathymetry and coastal orientation strongly affect the

* Corresponding author at: State Key Laboratory of Marine Environmental Science, Xiamen University, Xiamen 361005, Fujian, China. Tel.: +86 592 2185510; fax: +86 592 2185570.
E-mail address: ywjiang@xmu.edu.cn (Y. Jiang).

1463-5003/$ - see front matter © 2013 Elsevier Ltd. All rights reserved.
http://dx.doi.org/10.1016/j.ocemod.2013.06.004

upwelling frequency and intensity off coastal regions (Narimousa and Maxworthy, 1986; Song and Haidvogel, 1993; Torres et al., 2003; Gomez-Gesteira et al., 2008). Rodrigues and Lorenzzetti (2001), Song et al. (2001), and Song and Chao (2004) all suggested that it was necessary to combine the effects of wind stress together with bottom slope for studying coastal upwelling systems. Estrade et al. (2008) concluded that a steep shelf favored narrow cross-shore width of surface Ekman divergence (WSED), while a gradual shelf favored broad WSED. A gradual shelf slope concentrates the onshore nutrient transport in the bottom boundary layer, while a steeper shelf slope increases the interior transport between the surface and bottom boundary layers (Jacox and Edwards, 2011). Further, a poleward alongshore undercurrent will develop only over steeply sloped shelves (Choboter et al., 2011).

With respect to the upwelling off the California coast, the SST image (Fig. 1(a)) clearly shows that the coastal upwelling, which often extends several hundred kilometers from the coast from mid-March to mid-October, is the dominant physical process (Breaker and Mooers, 1986). By comparison, it is much weaker with a cold band ~25 km off the New Jersey coast (Fig. 1(b)), in spite of the fact that the dominant wind is upwelling favorable during summer. The upwelling often stays in stage (1) that subsurface water advects onshore off New Jersey coast, while upwelling further develops in stage (2) off California coast. The less frequent and less intense upwelling off New Jersey can be attributed to the higher intermittency of the upwelling-favorable wind (Smith, 1968) and the more gradual shelf slope, both of which are important factors that restrict the strength of coastal upwelling circulations (Garvine, 2004). The bathymetry off the New Jersey coast shows that the shelf has roughly an order of magnitude lower bottom slope than that off the California coast (Clarke and Brink, 1985; Lentz and Trowbridge, 1991; Garvine, 2004). Typical bottom slopes off the California coast are $\sim 1 \times 10^{-2}$, whereas the shelf bathymetry off the New Jersey coast is characterized by a more gradual slope $\sim 1 \times 10^{-3}$.

Fig. 2(a) and (b) shows the stick diagrams of wind velocity obtained from National Data Buoy Center (NDBC; buoy 46027 and 44009, indicated by the black squares in Fig. 1(a) and (b)) off each coast. The wind stress is decomposed to alongshore and cross-shore components. The alongshore component direct determining offshore Ekman transport is plotted in Fig. 2(c) and (d). Upwelling favorable winds are prevalent off the California coast with typical event durations of approximately one week, while the wind direction shifts back and forth off the New Jersey coast, with the upwelling favorable wind events lasting only 2–3 days (Jiang et al., 2012). In addition, the wind is much weaker and more variable in its direction off the New Jersey coast than those off the California coast. Since the wind forcing drives the coastal upwelling circulation, its strength and duration play dominant roles in determining the spatial extent of cold water. The bottom bathymetry can act to influence the upwelling process through the effect of bottom friction. As a result, we address the question of the relative importance of the wind forcing and the shelf slope in controlling the upwelling characteristics off the California and New Jersey coasts. In addition, it is also very important to fully explain the remarkable difference in the responses of these two upwelling systems.

This paper is organized as follows: The idealized numerical model is introduced in Section 2. In Section 3, the model is applied with spatially uniform wind fields to simulate the coastal upwelling processes for several idealized bottom bathymetries. As a concept to describe the tendency of cold upwelling areas, the theory of advection time is extended to include climbing and upwelling time scales, which are quantified through the use of a Lagrangian particle method within the numerical model. A discussion of the results is presented in Section 4, followed by conclusions in Section 5.

2. Numerical model

The numerical model used for the idealized simulations of the upwelling response to different wind and shelf slopes is the Regional Ocean Modeling System (ROMS) model (Shchepetkin and McWilliams, 2005). ROMS is a three-dimensional, hydrostatic, primitive equation ocean model which uses a stretched, generalized, terrain-following σ coordinate (Song and Haidvogel, 1994) and a horizontal, orthogonal, curvilinear Arakawa C-grid scheme. The model is configured with land on the western boundary, and the boundary conditions are periodic in the north and south, and outwardly radiative on the open eastern boundary. The turbulence closure scheme used is the Mellor-Yamada level-2.5 (MY-2.5) turbulence kinetic energy scheme. A third-order, upstream-biased horizontal advection scheme is used for the tracer and momentum equations, and a logarithmic bottom drag is assumed to calculate the bottom friction. The horizontal model domain is 225 km cross-shore with 0.5 km resolution, and two grid points in the alongshore direction. The minimum water depth is set to 5 m at the coast, and the bathymetry gradually descends to 200 m with a constant slope and rapidly drops to 250 m by the outer boundary to represent the continental slope (Fig. 3). The model is divided into 25 vertical terrain-following σ-levels, where $\theta_s = 3.0$, $\theta_b = 0.4$ and $h_c = 5$ m indicate that more grid points are concentrated near the surface (Fig. 3). The model uses an f-plane approximation with a Coriolis parameter of $f = 10^{-4}\ s^{-1}$. The initial velocities and surface elevation are set to zero, and the temperature is initialized in the whole model domain in the form:

$$T(z) = \frac{\pi}{2} \arctan\left(\frac{z+17}{5}\right) + 20, \tag{1}$$

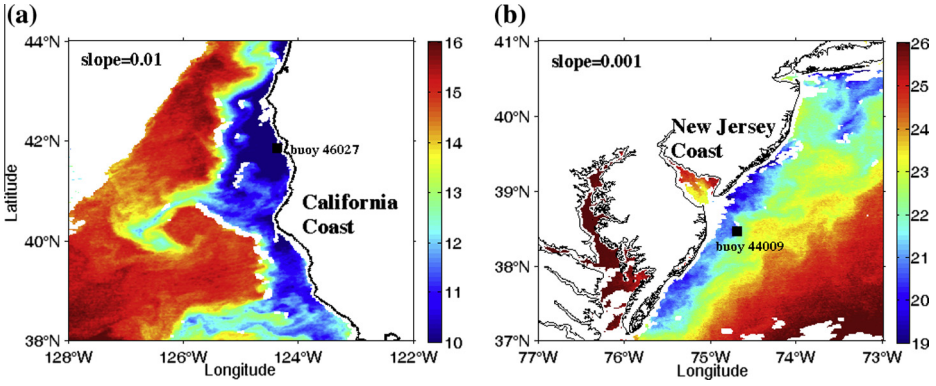

Fig. 1. MODIS SST (°C) (a) off the California coast on 25 June, 2003, and (b) off the New Jersey coast on 25 August, 2003. Wind measurements from NDBC are marked by black squares. Typical shelf slope is $\alpha = 10^{-2}$ for California, and $\alpha = 10^{-3}$ for New Jersey.

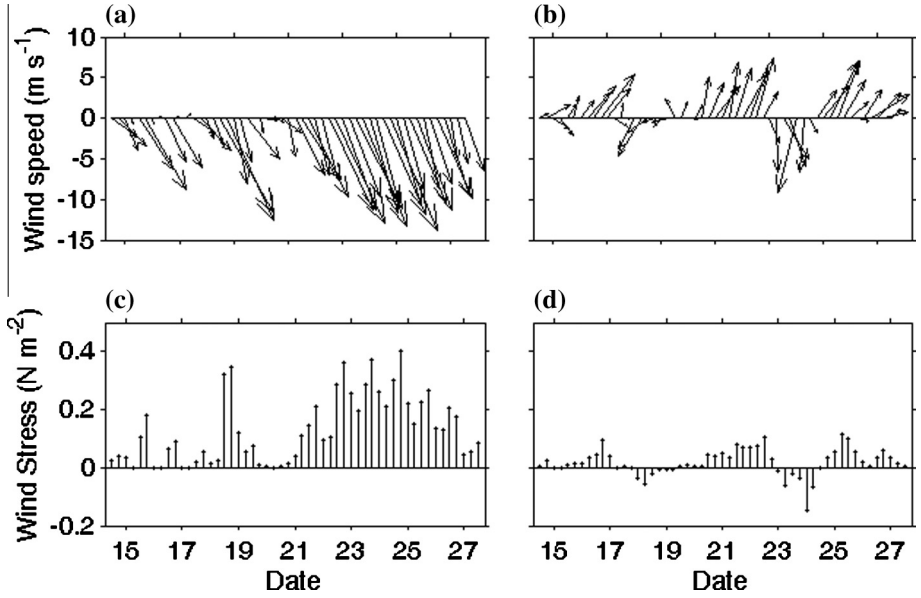

Fig. 2. Stick diagrams of wind velocity (m s^{-1}) from the NDBC buoys (a) for the California coast, 14–28 June, 2003, and (b) for the New Jersey coast, 14–28 August, 2003. (c) and (d) are the corresponding alongshore components (N m^{-2}). Positive value means an upwelling favorable wind direction.

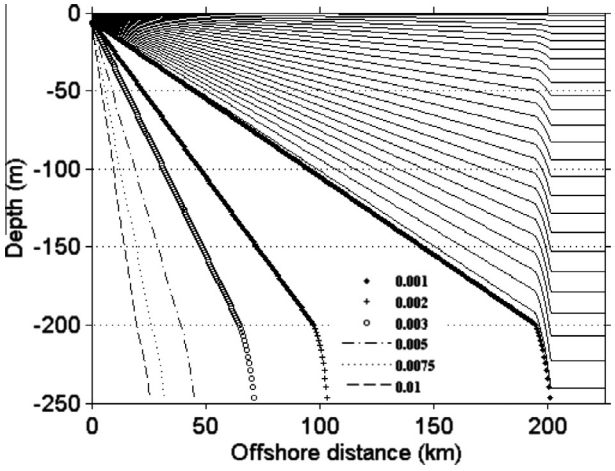

Fig. 3. Different shelf slopes in the numerical model experiments. Black solid lines denote σ-levels distribution for the case of slope $\alpha = 1.0 \times 10^{-3}$.

where z is the depth in meters. The temperature decreases from 22 °C at the surface to 20 °C at 17 m depth, and is nearly constant (~17.7 °C) below 50 m depth. The thermocline is located at 17 m. No heat or water mass fluxes are input at the air-sea interface, and the tidal processes are not included in the model. The initially stationary ocean is forced by spatially-uniform wind blowing from south to north, which gradually increases according to $\tau(t) = \tau_0(1 - e^{-3t})$, where t is the time in days, τ_0 is the alongshore wind stress. The wind reaches 95% of τ_0 in one day. The results were used for analysis after the model was run for 10 days.

3. Results

3.1. Model experiment schemes and results

Since the bathymetry and wind conditions are strikingly different off the east and west coasts of the U.S., the numerical model is run with different bottom slopes and wind stresses to check their effects on the wind-driven coastal upwelling system. To examine the effect of bathymetry, alongshore wind stress τ_0 is set to 0.05 N m^{-2}, which is typical alongshore wind forcing off the New Jersey coast in summer (Fig. 2(d)), and six cases are run with shelf slopes $\alpha = 10.0 \times 10^{-3}$, 7.5×10^{-3}, 5.0×10^{-3}, 3.0×10^{-3}, 2.0×10^{-3}, and 1.0×10^{-3} (Fig. 3). To examine the effect of wind, six cases with a constant slope $\alpha = 1.0 \times 10^{-3}$ and different wind stresses are run, corresponding to $\tau = 0.01$, 0.025, 0.05, 0.1, 0.15 and 0.2 N m^{-2}. No cross-shore wind and Ekman pumping effects are considered in any of the case studies.

Because the parameters of the numerical model are invariable in alongshore direction, and the model is expected to be two-dimensional. Cross-shelf profiles of the cross-shore velocity U, vertical velocity W and temperature T on day 10 are presented in Fig. 4 with MY-2.5 eddy viscosity profile. Taking the case of wind stress $\tau = 0.05$ N m^{-2}, slope $\alpha = 1.0 \times 10^{-3}$ as a reference case (Fig. 4(d)–(f)), the U field shows that the wind-driven, offshore transport occurs in the upper 20 m of the water column, with the onshore return flow mostly occurring in the bottom Ekman boundary layer. The return current interacts with the surface Ekman offshore flow on the inner-shelf within 30 km of the coast. The inner-shelf is defined as the transition region where the surface and bottom Ekman layers interact (Lentz, 1995). The shallow water effect over the inner-shelf causes a decrease of the surface Ekman layer thickness. The offshore current intensifies at 15 km offshore to approximately 0.05 m s^{-1}. The onshore return flow is approximately 0.02 m s^{-1} and 20 m thickness, which translates to an upslope current with large vertical velocity near the bottom. The sea surface level is low near the coast, and increases offshore. The sea level change caused by the surface offshore Ekman transport yields a pressure gradient directed westwards that generates a northward geostrophic alongshore current (not shown). As a consequence of the onshore return flow, the 20 °C isotherm lifts from the thermocline, and intersects the surface producing an extensive upwelling area next to the coast. The minimum SST appears at a location of 15 km offshore, and the cold water further drifts offshore and mixes with the surface warm water producing an upwelling front at 30 km off the coast.

An order of magnitude steeper shelf slope ($\alpha = 1.0 \times 10^{-2}$) yields the same magnitude of cross-shore velocity U, but the seaward boundary of inner-shelf is closer to the coast (Fig. 4(a)). Outside of the inner-shelf, the surface and bottom Ekman layers are

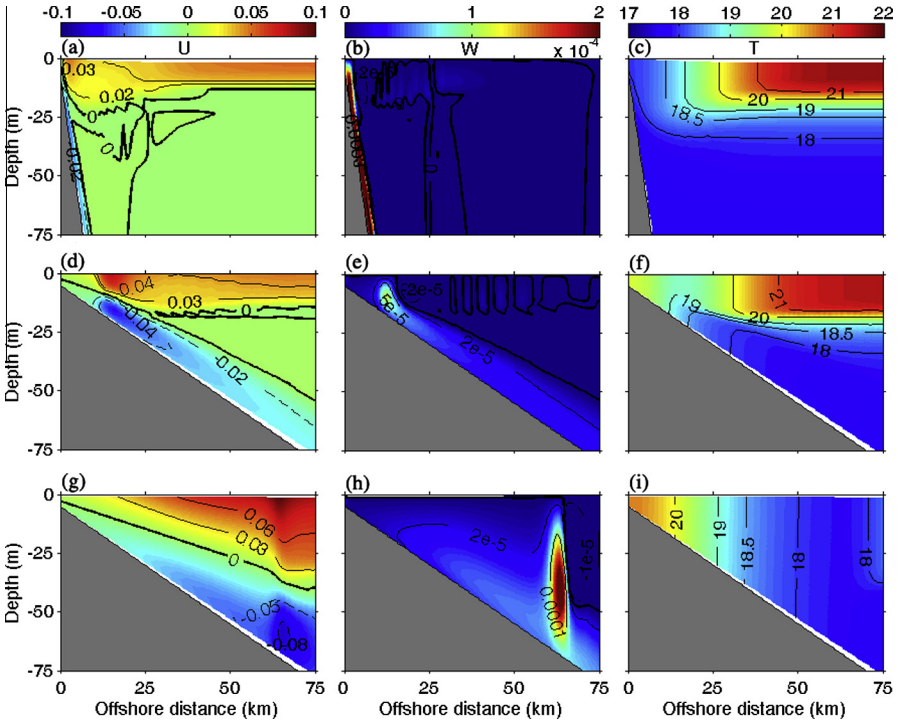

Fig. 4. Cross-shore profiles of the cross-shore velocity U (m s^{-1}), vertical velocity W (m s^{-1}) and temperature T (°C) from the numerical model. (a)–(c) for slope $\alpha = 10^{-2}$, wind stress $\tau = 0.05$ (N m^{-2}), (d)–(f) for slope $\alpha = 10^{-3}$, wind stress $\tau = 0.05$ (N m^{-2}), (g)–(i) for slope $\alpha = 10^{-3}$, wind stress $\tau = 0.2$ (N m^{-2}).

well separated, and no cross-shore flow is observed between them. In contrast to the cross-shore velocity, the vertical velocity is much more sensitive to the shelf slope (Fig. 4(b)). The W is one order of magnitude larger, and leads to a narrower band of return current and the location of the maximum in vertical velocity closer to the coast. Consequently, colder water is found in the nearshore (Fig. 4(c)).

In the case of stronger wind forcing ($\tau = 0.2$ N m^{-2}), the surface mixed layer thickens to roughly 40 m, and the width of the inner-shelf region is broader (Fig. 4(g)). The maximum cross-shore velocities increase in strength and occur further offshore at 65 km, with maximum offshore velocity in the surface layer reaching $\sim$0.08 m s^{-1} and maximum onshore velocity in the bottom layer reaching $\sim$0.08 m s^{-1}. The upwelling core of deep, cold water, characterized by stronger vertical velocity, appears centered in a band of roughly 10 km width at 60 km offshore (Fig. 4(h)), where the minimum surface temperature occurs (Fig. 4(i)). The warm sea water near the coast is due to the upwelling shutting down over the inner shelf (Estrade et al., 2008). In this case, the coastal upwelling region extends over a larger area and possesses a lower water temperature compared to the conditions in the reference case.

Another significant factor influencing the upwelling response is the wind duration. The offshore distances of the upwelling front as a function of time after wind onset for 3 different cases are presented in Fig. 5. Taking the case with wind stress $\tau = 0.05$ N m^{-2}, slope $\alpha = 1.0 \times 10^{-3}$ as a reference, it takes roughly 5.5 days for the 20 °C isotherm ($\Delta T = 2$ °C drop from the initial surface temperature) to outcrop to the surface. The 20 °C isotherm first outcrops at roughly 15 km offshore and then slowly migrates offshore at a speed of $\sim$4 km/day. For the stronger wind stress case, $\tau = 0.2$ N m^{-2}, it only takes $\sim$1.75 days for the 20 °C isotherm to outcrop, and it initially does so further offshore ($\sim$25 km). The offshore propagation speed of the upwelling front is $\sim$10 km/day, approximately 2.5 times the speed in the reference case. In the steeper shelf case, $\alpha = 1.0 \times 10^{-2}$, 20 °C water appears at the surface near the coast after $\sim$2 days, and thereafter moves offshore with roughly the same speed as in the reference case. Therefore, the location where the isotherm outcrops and the time required to transport the subsurface water to the surface are related to both the shelf slope and the strength of the wind stress, while the migration speed of the upwelling front is controlled by the strength of the wind stress alone. In particular, the longer and stronger the upwelling favorable winds exist, the larger will be the cold upwelling area. This result is similar to Breaker and Mooers (1986) finding that there is a strong correlation between the extent of the cold upwelling area and the time-integrated wind stress.

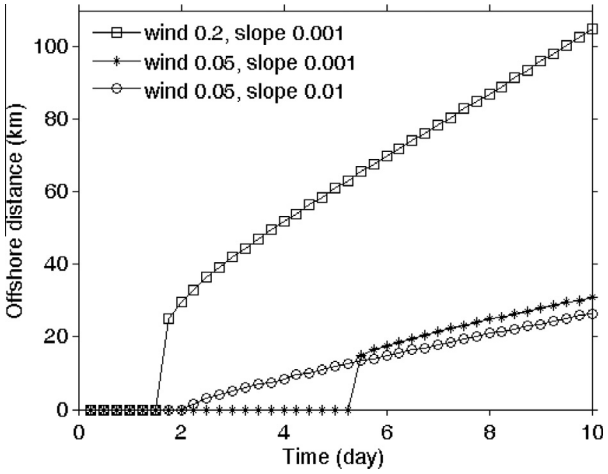

Fig. 5. Time evolution of offshore positions of the upwelling front in different cases, defined as $\Delta T = 2$ °C.

While the upwelling conditions are more favorable in the California upwelling system (typical values of slope $\alpha = 10^{-2}$, wind stress $\tau = 0.2$ N m^{-2}, wind duration $t = 7$ days) than those off the

New Jersey coast (typical values of slope $\alpha = 10^{-3}$, wind stress $\tau = 0.05$ N m^{-2}, wind duration $t = 2$ days), it is not immediately clear whether the role of wind forcing is more important than shelf slope for these two upwelling systems. To answer this question, we exchange the wind conditions in these two coastal areas. Fig. 6(a) shows the cross-shore profile of temperature that a typical wind event off the California coast would induce if it had occurred off the New Jersey coast instead. The cold subsurface water uplifts along the shelf, and presents a large cold upwelling area on the surface. Conversely, Fig. 6(b) shows the cross-shore profile of temperature that a typical wind event off the New Jersey coast would induce if it had occurred off the California coast. In this case, upwelling is weak off the coast. Together, these results indicate that the role of wind is more important than the shelf slope in the upwelling systems off the California and New Jersey coasts.

3.2. Particles release experiment and advection time

The cold upwelling areas are strikingly different off these two upwelling regions, especially the fact that upwelling infrequently occurs off the New Jersey coast. One reason is the typically shorter duration of the upwelling favorable winds combined with the longer advection time needed to bring the cold, subsurface water all the way to the surface. The numerical model results reveal that the time scale for 20 °C isotherm outcropping varies under different wind and slope conditions (Fig. 5) as described above. Fig. 7(a) gives a schematic for advection time, i.e. the time for the cold water advecting from pycnocline to coast (Jiang et al., 2012). The bottom cross-shore speed $u = M/d = \tau/(\rho f d)$, where M is the Ekman transport, d is the bottom layer thickness, τ is the wind stress, ρ is the water density, and f is the Coriolis parameter. Then the advection time is $t_{ad} = (H_0 - H_1)/(\alpha u)$, and is given by:

$$t_{ad} = \frac{\rho f d (H_0 - H_1)}{\alpha \tau}, \tag{2}$$

where H_0 is the depth of pycnocline, H_1 is the water depth achieved by advection process, and α is the shelf slope. This equation gives a theoretical estimate of the advection time detailing the dependence on the bottom slope and wind stress intensity. When the time duration of the upwelling favorable wind is less than the advection time, the cold water cannot be transported all the way to the surface, so the upwelling region will not appear. Considering the cross-shore profiles of U, W and T (Fig. 4), we find that the upwelling process consists of two phases, (1) the up-climbing phase where the isopycnals move up along the shelf bottom and (2) the upwelling phase after they separate from the bottom. Therefore, it is important to identify the depth where these two processes separate so that we can modify Eq. (2) to include an upwelling time scale term.

To simplify the problem, we run the numerical model with a constant eddy viscosity $A_z = 3.5 \times 10^{-3}$ m^2 s^{-1} (Souza et al., 2004). We release 500 passive particles at 17 m depth from 11.7 km to 36.7 km offshore. This initial depth is determined by the location of thermocline according to Eq. (1), and the corresponding temperature is 20 °C. The particles are initially evenly distributed across the 50 grid cells aligned offshore from the shelf. The alongshore migration is set to zero to ensure that the particles do not leave the model domain. No random walk component is introduced in the experiment, so that the movements of the particles are controlled by the advection. The positions of the particles are stored hourly. Considering a case with a wind stress of $\tau = 0.1$ N m^{-2} and a bottom slope of $\alpha = 1.0 \times 10^{-3}$ as an example, Fig. 8 shows the positions of the floats and the 20 °C isotherms at different wind duration time. The dome-shaped 20 °C isotherm uplifts along the shelf within the first 5 days. After that, upwelling appears on the surface with 20 °C isotherm outcropping and shifting offshore forced by the continual wind on the surface. Because of

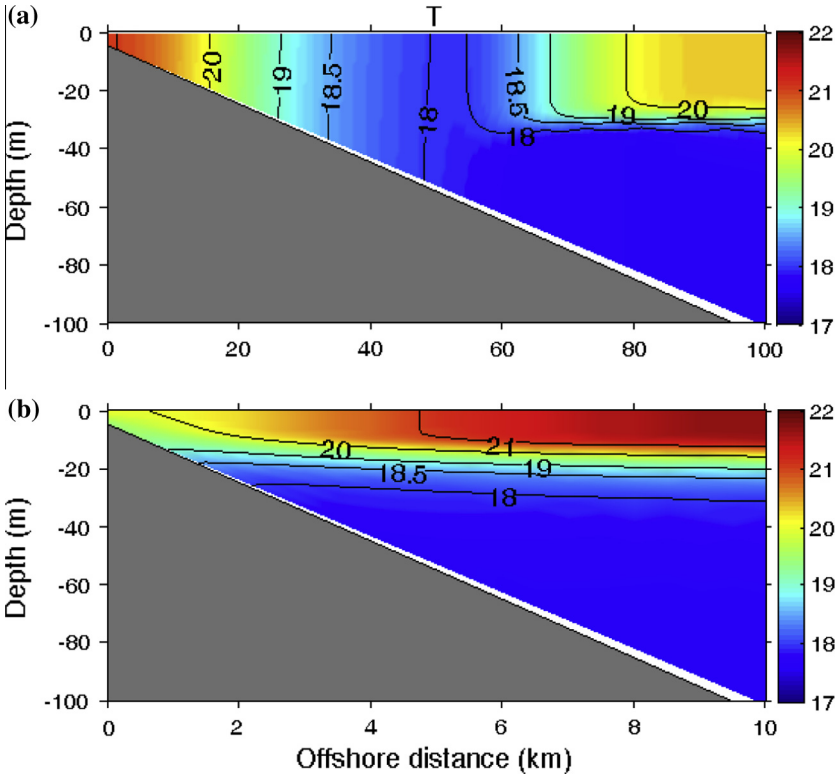

Fig. 6. Cross-shore profiles of the temperature T (°C) from the numerical model. (a) for slope $\alpha = 10^{-3}$, wind stress $\tau = 0.2$ (N m^{-2}), wind blowing 7 days, (b) for slope $\alpha = 10^{-2}$, wind stress $\tau = 0.05$ (N m^{-2}), wind blowing 2 days.

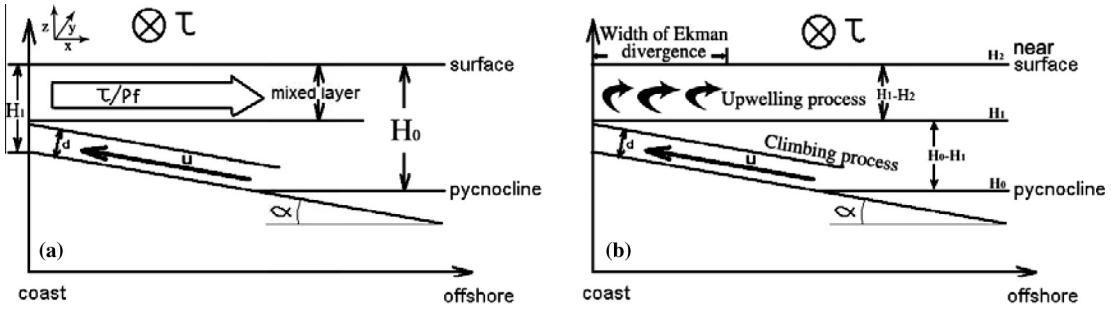

Fig. 7. Schematics for the advection time t_{ad}, (a) proposal from Jiang et al. (2012); (b) Eq. (3) of this study.

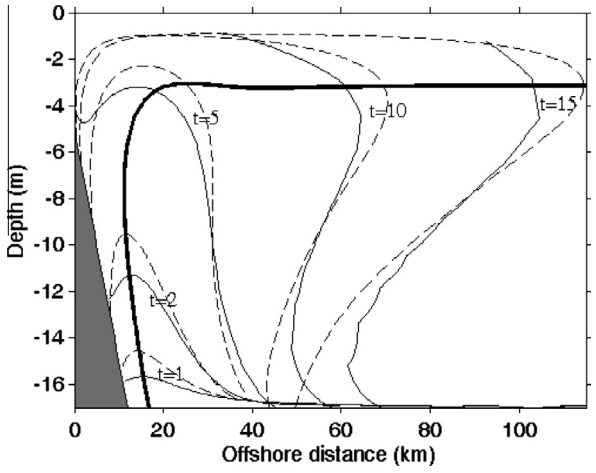

Fig. 8. Temporal evolution of the floats (dashed line) released at 17 m and the 20 °C isotherms (solid line) (unit: day). Thick line is the trajectory of the fastest particle.

the diffusion processes, the water particles originated from the thermocline are warmer (colder) than 20 °C along the upwelling channel, resulting in the 20 °C isotherm behind (before) to the positions of the floats at the front (two wings). The friction and horizontal diffusion make the water temperature near bottom shelf closer to the upwelling cell. Although the diffusion processes affect the water temperature pattern to some extent, the advection process dominates the coastal upwelling circulation in the transport of cold water. Therefore, the time scale of the floats advecting to the surface is approximate to that of thermocline outcropping.

Fig. 9 shows the Lagrangian cross-shore and vertical velocity fields derived from the trajectory of particles within the model after 15 days. First, the particles climb up the shelf, and then are transported offshore after they cross the region between the surface mixed layer and bottom Ekman layer. The particles near bottom shelf cover the surface after model runs for 15 days, while particles near geostrophic interior are advected in a short distance. The particles are still initially, and accelerate continuously along the shelf. After reaching a maximum value at ~12 m, they slow down because of the decrease of W up to the surface. The fastest particle, marked in thick line, tracks along the maximum vertical velocity for each z level in the "up-climbing" process, and only begins to deviate from it after crossing the location of the direction transition of cross-shore velocity. The fastest particle climbs up the shelf, advects onshore within the bottom friction layer, and then upwells and is transported offshore when it reaches the surface Ekman layer. Because the surface Ekman layer thickness is limited by the shallow water on the inner-shelf, the model results indicate that the switch-over depth for these two processes is located at approximately $0.9D_E$ ($D_E = \sqrt{2A_z/f}$ is the Ekman depth) and is independent of the shelf slope and the wind strength and duration under the assumption of constant eddy viscosity. Therefore, without the consideration of the effects of mixing and diffusion, Eq. (2) can be adjusted to be:

$$t_{ad} = \frac{\rho f d(H_0 - H_1)}{\alpha\tau} + \frac{H_1 - H_2}{W}, \tag{3}$$

where H_1 is the switch-over depth between the up-climbing and upwelling processes, $\sim 0.9D_E$, H_2 is the depth to which the fastest particle reaches after these two processes (also see Fig. 7(b) for the schematic), $d = \pi\sqrt{2A_z/f}$ is the bottom friction layer thickness, $W = \tau/(\rho f L)$ is the averaged vertical velocity over the upwelling region, and L is the length scale of WSED, which we take $L = 0.75\pi\sqrt{2A_z}/\left(\sqrt{f}\alpha\right)$ in this study (Estrade et al., 2008). The first

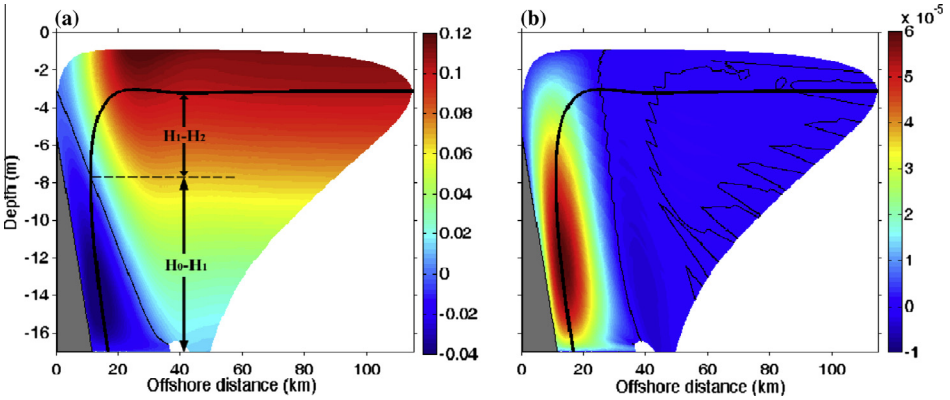

Fig. 9. (a) Cross-shore velocity U (m s^{-1}) and (b) vertical velocity W (m s^{-1}) calculated from the trajectory of the released particles. Thin line marks zero velocity, and thick line is the trajectory of the fastest particle. Dashed line describes the switch-over depth of the up-climbing and upwelling processes.

term is the climbing time scale, and later term relates to upwelling time scale. Both of these time scales are inversely proportional to shelf slope and intensity of wind stress. Note that we only consider the advection effect, the particle moving to the depth H_2 is regarded as having arrived at the sea surface. For simplicity, we define H_0 as the depth of thermocline rather than pycnocline, and take advantage of the fact that it is more convenient to observe the cold water appearing at the surface from the satellite images.

The numerical model with a constant eddy viscosity is used to validate the shelf slope and wind stress effects on the advection time as theorized in Eq. (3). Since the eddy viscosity is a constant, H_1 is invariant $\sim 0.9D_E$ in all cases, and we find $H_2 = 0.35D_E$, ~3 m based on the particle release experiments. The climbing and upwelling times are determined by time for the 20 °C isotherm uplifting from H_0 (thermocline depth) to H_1 (transition depth), and H_1 to H_2, respectively. The dependence of the climbing and upwelling times on different slopes and wind stress intensities are shown in Fig. 10. Wind stress is fixed to 0.05 N m^{-2} when checking the slope effect (Fig. 10(a)), and slope is fixed to 10^{-3} when checking the wind effect (Fig. 10(b)). The results from the numerical simulations (closed symbols) agree reasonable well with the theoretical values calculated from Eq. (3) (open symbols), and show approximately an inverse proportionality to both shelf slope and wind stress intensity. The relationships in numerical model results are not as strictly linear as that derived from Eq. (3), which may be due to the model spin-up and diffusion processes, e.g. the weaker the wind stress, more time the spin-up process needs. Gradual shelf slope and weaker wind stress both lead to larger climbing and upwelling advection times, meaning that a longer duration of upwelling favorable winds is needed to advect the cold water all the way to the surface. Comparing the climbing time (circles) to the upwelling time (triangles) shows that the majority of the total advection time is spent on climbing the slope, and these times are related to the vertical velocity and the thickness of surface Ekman layer on the inner-shelf. Note that Eq. (3) is only an estimate of the advection time; numerical models and observations are needed to further obtain an exact advection time in specific upwelling regions.

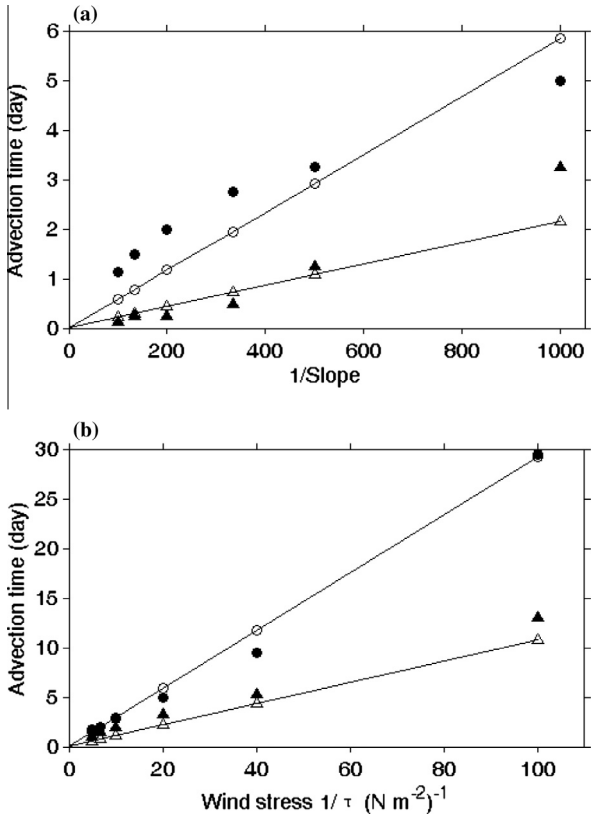

Fig. 10. Advection time in (a) different slopes and (b) different wind stress conditions: climbing advection time (circles), and upwelling advection time (triangles), where closed signs for numerical model, and open signs for theoretical values. The eddy viscosity is a constant in all the cases ($A_z = 3.5 \times 10^{-3}$ m^2 s^{-1}).

4. Discussion

Using an analytic solution, Estrade et al. (2008) pointed out that the scale of the WSED was $L = 0.75\pi\sqrt{2A_z}/\left(\sqrt{f}\alpha\right)$. To examine the relationship between L and wind strength, we average the exponential eddy viscosity profile (Long, 1981; Lentz, 1995) in a scale of turbulent boundary layer δ to determine a typical value:

$$A_z = \frac{\int_0^{\delta} ku^* z' \exp\left(\frac{-z'}{l}\right) dz'}{\delta}, \tag{4}$$

where $\delta = ku^*/f$, $k = 0.4$ is the Von Karman constant, $u^* = \sqrt{\tau/\rho}$ is the shear velocity, z' is the distance from the boundary, and $l = 0.27\delta$ is the exponential decay scale. From Eq. (4), it can be found the eddy viscosity $A_z \approx 0.01\tau/(\rho f)$, meaning $A_z \propto \tau$. Then, the WSED is proportional to $\sqrt{\tau}$ and $1/\alpha$. This implies that greater wind strength and gentle shelf slope correspond to larger WSED. We hypothesize that the upwelling process is two-dimensional, the volume of the upwelled water must be exactly equal to the offshore transport. Consequently, the averaged vertical velocity within the WSED is given by $\overline{W} = M/L = \tau\alpha/\left(0.75\pi\rho\sqrt{2fA_z}\right)$. In this case, $\overline{W}$ is proportional to α and $\sqrt{\tau}$. This implies that vertical velocity is positively correlated to shelf slope and wind strength. These are the reasons for the vertical velocity structures response to wind strength and shelf slope in Fig. 4. The theoretical expressions of the WSED and vertical velocity are based on a constant eddy viscosity controlled by the wind stress. The eddy viscosity in the numerical model, calculated by the MY-2.5 turbulent closure scheme, is small in the geostrophic interior. The location and WSED are sensitive to the eddy viscosity profile, and the weaker eddy viscosity interior produces narrower WSED in shallower water comparing to the eddy viscosity profiles with larger values (Lentz, 1995). Therefore, the theoretical values given by a constant eddy viscosity averaged in the whole water column will overestimate the WSED, and underestimate the vertical velocity.

The model experiments show that stronger wind stress, steeper bottom slope, and longer wind duration result in upwelling events with a larger vertical velocity and more extensive cold water area. Therefore, the vertical velocity is expected to be larger in the California upwelling system than in that off the New Jersey coast. Off the California coast, the stronger wind stress acts to increase the WSED, whereas the steeper bottom slope acts to decrease it. The large area of cold water off the California coast observed in satellite images can be attributed to stronger wind stress, longer wind duration and steeper bottom slope, which lead to shorter advection time. Stronger wind stress drives a larger offshore transport, which leads to an upwelling front that is further offshore (Fig. 4(i) vs. (f)). With respect to the effect of shelf slope, it takes a longer time for the subsurface water to advect to the surface over a gradual slope because of the longer advection distance and smaller vertical velocity. After the cold water outcrops, the propagation speed of the upwelling front, which is controlled by the magnitude of the transport in the surface Ekman layer, is independent of the shelf slope.

The variation and trend of upwelling north of off San Francisco on the U.S. west coast are positively related to the equatorward wind (Seo et al., 2012). The variations in SST caused by upwelling

off the central California are correlated with both changes in wind and the climate indices (García-Reyes and Largier, 2010). Off the New Jersey coast, the currents are significantly coherent with the wind with an offshore (onshore) flow in the upper (lower) layer when the wind is upwelling favorable (Wong, 1999). During an upwelling favorable wind pulse, cold water is brought to the surface through the bottom boundary layer in the manner of Ekman dynamics on the New Jersey shelf (Yankovsky, 2003). Therefore, the winds are the dominant effect on coastal upwelling processes in this two regions, although mesoscale eddies have influences on shaping the eastern boundary upwelling systems dynamical structure (Capet et al., 2008) and filament structure are dependent on local processes in the California Current System (Penven et al., 2006), the roles of which are beyond the extent of this study.

By late spring, coastal upwelling strengthens and reaches its maximum in June, weakens by late summer and ends in October. April–August is regarded as the spring-summer upwelling season (Huyer and Kosro, 1987). Off the New Jersey coast, the Bermuda/Azores high builds into the southeast by April, and southerly (upwelling favorable) winds are prevalent from May to September, while westerly and northwesterly (upwelling unfavorable) winds are prevalent in the winter (Klink, 1999). In upwelling season, the stratification is weak with deep pycnocline off the California coast, while it reverses off the New Jersey coast, but the Burger number is ~0.7 for both regions, indicating the similar effect of stratification in the subtidal frequency dynamics (Jiang et al., 2012). In periods of strong wind driven upwelling events, the alongshore wind stress is changeable in a range of −0.4 to 0.1 N m^{-2} (positive northward) with typical wind duration period of 7–10 days off the California coast (Huyer and Kosro, 1987). The wind stress has high-frequency variability in a range of −0.08 to 0.08 N m^{-2} with wind events period of 1–3 days off the New Jersey coast in May–August, 1996 (Yankovsky and Garvine, 1998). Jiang et al. (2012) used an idealized numerical model to estimate the advection time for both coasts and found it to be 0.5 days for the Oregon coast and 3 days for the New Jersey coast. It takes two days of upwelling-favorable wind to cause the pycnocline to outcrop off the New Jersey coast (Yankovsky, 2003), while the surface temperature and salinity respond to the variations of the alongshore wind within one day during upwelling events off the California coast (Huyer, 1984). It is important to note that the wind duration time often exceeds the advection time over the California shelf, but not over the New Jersey shelf in upwelling season. Thus the condition is more upwelling-favorable off the California coast than off the New Jersey coast. This tendency is quantified by the proxy of upwelling age. When it is less than 1, the upwelling front cannot form at the surface. If it exceeds 1, an upwelling area appears. The larger Γ is, the stronger upwelling tendency will be.

The results in Figs. 1 and 6 can be explained by upwelling age theory: the ratio of the wind duration in these two upwelling systems is 7:2, and that of wind stress intensity is 4:1. Since $t_{ad} \propto 1/\tau$, the ratio of the wind contribution to the upwelling age in these two upwelling systems is 14:1. While, the ratio of slope effect contributed to the upwelling age in these two upwelling systems is only 10:1, which is smaller than the wind effect. Consequently, the net ratio of upwelling age for the California and New Jersey upwelling systems is roughly 140:1, which explains the reason for the enormous difference between the extents of the cold upwelling areas off each coast observed in satellite SST images. Of course, for the New Jersey coast, the upwelling region will appear if the duration of upwelling favorable wind is long enough, rather than the wind direction shifting back and forth, although it is restricted by the wide and shallow continental shelf. Note that the linear relationship between the advection time and wind duration, wind stress, shelf slope is based on the assumption of the homogenous ocean in the idealized condition. The complicated coastline, bathymetry, eddies, currents, etc. will make the upwelling processes more intricate response to the wind and shelf, and this linear relationship shall be elaborated and modified.

The advection time in Eq. (3) is derived from one-dimensional Ekman theory, assuming a constant eddy viscosity. However, in the real ocean, eddy viscosity varies from surface to bottom within the range of 10^{-3} to 10^{-2} m^2 s^{-1} (Souza et al., 2004), and is influenced by wind stress, bottom stress, stratification, etc. The variations of magnitude and direction of the wind stress result in the change of the switch-over depth, H_1, and the vertical velocity. The interaction of the surface and bottom boundary layers and interactive response of wind-driven cross-shelf circulation to different topographic forcing are complex (Gan et al., 2009). Further, the bottom layer thickness, d, and bathymetry vary in different coastal areas, such as off the northwestern Africa, northern California, Oregon, and Peru (Smith, 1981). Therefore, it becomes more complicated to estimate the advection time in different upwelling regions. Meanwhile, the deeper pycnocline in winter will result in a larger climbing advection time. All of these factors influence the advection time in a real upwelling system. Nevertheless, Eq. (3) gives an estimate for the advection time consisting of climbing and upwelling processes, and shows the relative effects of shelf slope and wind stress. It is more difficult to advect the cold water to the surface (i.e. the advection time is larger) with weaker wind stress over gradually sloping shelf like that off the New Jersey coast. On the inner-shelf, because of limited water depth, the bottom and surface Ekman layers interact with each other. According to the idealized Lagrangian particle experiments, the cold subsurface water advects onshore to the inner-shelf until it reaches a depth of $\sim 0.9D_E$, where it is upwelled and then transported offshore. First, the kinetic energy of the wind is used to transport cold water from pycnocline to the surface, and there is no obvious temperature drop off the coastal region. After that, the remaining duration of upwelling favorable wind drives the upwelling front offshore and presents a cold upwelling area.

5. Conclusions

In this study, we compare the upwelling systems off the California and New Jersey coasts with regards to the contribution of wind stress intensity, wind duration and shelf slope to the different upwelling intensities in these two areas. An idealized numerical model simulation is used to study these effects on wind-driven coastal upwelling. The model results show that stronger wind stress leads to a deeper Ekman layer depth and a larger offshore velocity, which leads to the formation of a larger cold upwelling area, whereas, the bottom slope effect on them is negligible. Steep slope and weak wind lead to narrow WSED, while steep slope and great wind strength lead to large vertical velocity. For the case of strong wind stress over a gradual shelf slope, the maximum vertical velocity, and consequently the position where the isotherm first outcrops, appears farther from the coast.

We extend the definition of advection time, which is the main concept within upwelling age theory, to differentiate between climbing and upwelling time scales. Climbing time is the time scale for cold water to climb up the slope from the pycnocline to the depth where it leaves the bottom, and upwelling time is the time scale for the cold water to rise from the bottom to the surface. Both these time scales, expressed by Eq. (3), are inversely proportional to shelf slope and wind stress. Through Lagrangian particle release experiments in the idealized numerical model with constant eddy viscosity, we find that the switch-over depth for these two processes is located at $\sim 0.9D_E$. When the duration of wind forcing is less than the advection time scale, upwelling front will not appear

off the coast. If the duration of upwelling-favorable wind exceeds the advection time scale, isopycnals outcrop and an upwelling front is formed. The larger ratio of wind duration time to the advection time denotes stronger upwelling tendency. For steeper shelves, less advection time is needed because a shorter horizontal distance is required to transport cold water to the surface. The stronger wind stress increases the cross-shore velocity and Ekman transport, leading to a reduction of the advection time. Therefore, the expression of the "upwelling age", Γ, is:

$$\Gamma = \frac{t_{wind}}{t_{ad}} = \frac{t_{wind}}{\frac{\rho f d(H_0 - H_1)}{\alpha \tau} + \frac{H_1 - H_2}{W}}, \quad (5)$$

where t_{wind} is the upwelling favorable wind duration.

The California coastal region is considerably more favorable to the development of upwelling because of stronger wind stress, longer duration of upwelling favorable winds and a steeper shelf compared to conditions off the New Jersey coast. As an application of the model results and upwelling age theory, the exchanged wind forcing experiments show that a large cold upwelling area would appear off the New Jersey coast under California wind conditions, while much less cold water would upwell to the surface in the converse case of New Jersey wind conditions imposed off the California coast. These results indicate that the role of wind is the dominant factor in determining the upwelling intensity in these two areas. Further, the application of the upwelling age concept adequately explains the differences in upwelling features between the east and west coasts of the U.S. The less advection time results in upwelling phenomenon, as well as the related biological and chemical processes, rapider response to alongshore wind off the California coast. Although the roles of wind and topography on upwelling are studied to some extent about upwelling age here, the effects of eddy and filament transport, variable eddy viscosity and model spin-up processes on the advection time, and therefore upwelling age need further elaborate study.

Acknowledgments

This study was partially supported by NASA Physical Oceanography and EPSCoR Programs and by NOAA Sea Grant in U.S.; by 973 Program (2009CB421200, 2013CB955700) from the National Basic Research Program of China, and by the Natural Science Foundation of China (Grant No. 41076001), and the Fundamental Research Funds for the Central Universities (Grant No. 2010121029) in China. We would like to thank R.W. Garvine and L.C. Breaker for the initial idea on the comparison of upwelling off the eastern and western U.S. coasts in an early collaborative NSF proposal. We also thank the two anonymous reviewers for helpful comments on the manuscript.

References

Allen, J.A., Newberger, P.A., Federick, J., 1994. Upwelling circulation on the Oregon continental shelf, part 1: response to idealized forcing. Journal of Physical Oceanography 25, 1843–1866.

Breaker, L.C., Mooers, C.N.K., 1986. Oceanic variability off the central California coast. Progress in Oceanography 17, 61–135.

Capet, X., Colas, F., McWilliams, J.C., Penven, P., Marchesiello, P., 2008. Eddies in eastern boundary subtropical upwelling systems. In: Hecht, M.W., Hasumi, H. (Eds.), Ocean Modeling in an Eddying Regime, Geophysical Monograph Series, vol. 177. AGU, Washington, DC, pp. 131–147. http://dx.doi.org/10.1029/177GM10.

Choboter, P.F., Duke, D., Horton, J.P., Sinz, A.P., 2011. Exact solutions of wind-driven coastal upwelling and downwelling over sloping topography. Journal of Physical Oceanography 41, 1277–1296.

Clarke, A.J., Brink, K.H., 1985. The response of stratified, frictional flow of shelf and slope waters to fluctuating large-scale, low-frequency wind forcing. Journal of Physical Oceanography 15, 439–453.

Estrade, P., Marchesiello, P., Verdière, A.C.D., Roy, C., 2008. Cross-shelf structure of coastal upwelling: a two-dimensional extension of Ekman's theory and a mechanism for inner shelf upwelling shut down. Journal of Marine Research 66, 589–616.

Gan, J., Cheung, A., Guo, X., Li, L., 2009. Intensified upwelling over a widened shelf in the northeastern South China Sea. Journal of Geophysical Research 114, C09019. http://dx.doi.org/10.1029/2007JC004660.

García-Reyes, M., Largier, J., 2010. Observations of increased wind-driven coastal upwelling off central California. Journal of Geophysical Research 115, C04011. http://dx.doi.org/10.1029/2009JC005576.

Garvine, R.W., 2004. The vertical structure and subtidal dynamics of the inner shelf off New Jersey. Journal of Marine Research 62, 337–371.

Gomez-Gesteira, M., Castro, M., Alvarez, I., Lorenzo, M.N., Gesteira, J.L.G., Crespoa, A.J.C., 2008. Spatio-temporal upwelling trends along the Canary Upwelling System (1967–2006). Trends and Directions in Climate Research 1146, 302–337. http://dx.doi.org/10.1196/annals.1446.004.

Huyer, A., 1984. Hydrographic observations along the CODE central line off northern California, 1981. Journal of Physical Oceanography 14, 1647–1658.

Huyer, A., Kosro, P.M., 1987. Mesoscale surveys over the shelf and slope in the upwelling region near Point Arena, California. Journal of Geophysical Research 92, 1655–1681.

Jacox, M.G., Edwards, C.A., 2011. Effects of stratification and shelf slope on nutrient supply in coastal upwelling regions. Journal of Geophysical Research 116, C03019.

Jiang, L., Yan, X.-H., Tseng, Y.-H., Breaker, L.C., 2011. A numerical study on the role of wind forcing, bottom topography, and nonhydrostacy in coastal upwelling. Estuarine Coastal and Shelf Science 95 (1), 99–109. http://dx.doi.org/10.1016/j.ecss.2011.08.019.

Jiang, L., Yan, X.-H., Breaker, L.C., 2012. Upwelling age – an indicator of local tendency for coastal upwelling. Journal of Oceanography 68, 337–344. http://dx.doi.org/10.1007/s10872-011-0096-2.

Klink, K., 1999. Climatological mean and interannual variance of United States surface wind speed, direction and velocity. International Journal of Climatology 19, 471–488.

Lentz, S.J., 1995. Sensitivity of the inner-shelf circulation to the form of the eddy viscosity profile. Journal of Physical Oceanography 25, 19–28.

Lentz, S.J., Trowbridge, J.H., 1991. The bottom boundary-layer over the Northern California shelf. Journal of Physical Oceanography 21, 1186–1201.

Long, C.E., 1981. A simple model for time-dependent stably stratified turbulent boundary layers, Tech. Rep. Special Report, No. 95, pp. 170, University of Washington, Seattle, Washington.

Melton, C., Washburn, L., Gotschalk, C., 2009. Wind relaxations and poleward flow events in a coastal upwelling system on the central California coast. Journal of Geophysical Research 114, C11016. http://dx.doi.org/10.1029/2009JC005397.

Narimousa, S., Maxworthy, T., 1986. Coastal upwelling on a sloping bottom: the formation of plumes, jets and pinched-off cyclones. Journal of Fluid Mechanics 176, 169–190.

Penven, P., Debreu, L., Marchesiello, P., McWilliams, J.C., 2006. Evaluation and application of the ROMS 1-way embedding procedure to the central California upwelling system. Ocean Modelling 12 (1–2), 157–187.

Pringle, J.M., Dever, E.P., 2009. Dynamics of wind-driven upwelling and relaxation between Monterey Bay and Point Arena: local-, regional-, and gyre-scale controls. Journal of Geophysical Research 114, C07003. http://dx.doi.org/10.1029/2008JC005016.

Rodrigues, R.R., Lorenzzetti, J.A., 2001. A numerical study of the effects of bottom topography and coastline geometry on the Southeast Brazilian coastal upwelling. Continental Shelf Research 21, 371–394.

Seo, H., Brink, K.H., Dorman, C.E., Koracin, D., Edwards, C.A., 2012. What determines the spatial pattern in summer upwelling trends on the U.S. West Coast? Journal of Geophysical Research 117, C08012. http://dx.doi.org/10.1029/2012JC008016.

Shchepetkin, A.F., McWilliams, J.C., 2005. The regional ocean modeling system: a split-explicit, free-surface, topography-following coordinates ocean model. Ocean Modelling 9, 347–404.

Smith, R.L., 1968. Upwelling. In: Barnes, H. (Ed.), Oceanography and Marine Biology: An Annual Review, vol. 6. G. Allen & Unwin, London, pp. 11–46.

Smith, R.L., 1981. A comparison of the structure and variability of the flow field in three coastal upwelling regions: Oregon, Northwest Africa, and Peru. In: Coastal Upwelling. American Geophysical Union, pp. 107–118.

Song, Y.T., Chao, Y., 2004. A theoretical study of topographic effects on coastal upwelling and cross-shore exchange. Ocean Modelling 6, 151–176. http://dx.doi.org/10.1016/S1463-5003(02)00064-1.

Song, Y.T., Haidvogel, D.B., 1993. Numerical simulations of the CCS under the joint effects of coastal geometry and surface forcing. In: Spaulding, M.L. et al. (Eds.), Estuarine and Coastal Modeling. American Society of Civil Engineers, Reston, VA, pp. 216–234.

Song, Y.T., Haidvogel, D.B., 1994. A semi-implicit ocean circulation model using a generalized topography following coordinate system. Journal of Computational Physics 115, 228–244.

Song, Y.T., Haidvogel, D.B., Glenn, S., 2001. The effects of topographic variability on the formation of upwelling centers off New Jersey: a theoretical model. Journal of Geophysical Research 106 (C5), 9223–9240.

Souza, A.J., Alvarez, L.G., Dickey, T.D., 2004. Tidally induced turbulence and suspended sediment. Geophysical Research Letters 31, L20309. http://dx.doi.org/10.1029/2004GL021186.

Torres, R., Barton, E.D., Miller, P., Fanjul, E., 2003. Spatial patterns of wind and sea surface temperature in the Galician upwelling region. Journal of Geophysical Research 108, 3130–3143. http://dx.doi.org/10.1029/2002JC001361.
Wong, K.-C., 1999. The wind driven currents on the Middle Atlantic Bight inner shelf. Continental Shelf Research 19, 757–773.
Yankovsky, A.E., 2003. The cold-water pathway during an upwelling event on the New Jersey shelf. Journal of Physical Oceanography 33, 1954–1966.
Yankovsky, A.E., Garvine, R.W., 1998. Subinertial dynamics on the inner New Jersey shelf during the upwelling season. Journal of Physical Oceanography 28, 2444–2458.